ADVANCED ENERGY MATERIALS
www.advenergymat.de

Separating Nucleation and Growth: High-Overpotential Pretreatment Pulses for Sodium-Metal Electrodes

Meghdad Hosseinzadegan, Felix Bauer, Leif Nyholm, Guiomar Hernández, and David R Maibach**

Sodium metal is capable of unlocking a new sustainable pathway toward electrification thanks to its high energy density and abundant resources. However, uneven metal nucleation and growth during cycling remains a challenge to be fully understood and overcome. In this study, short high-overpotential pretreatment pulses are applied to enable 2D metal growth. This is achieved by separating the initial nucleation step from reversible sodium metal growth. Electrochemical measurements combined with scanning electron microscopy and image analysis prove that the reductive and oxidative pulses significantly decrease the initial overpotential during galvanostatic cycling, compared to cycling without pulses. The oxidative or reductive pulses activate the entire electrode surface by generating a dense population of single micrometer-sized pits or nuclei, respectively. This activation of the surface decreases the interfacial impedance and circumvents the generation of mossy sodium and forms a smooth hill-valley-like topography. Double pulse pretreatment further improves the 2D sodium growth. This improvement is also seen in full-cells with Prussian white as the cathode material as an increase in Coulombic efficiency. The results of this study demonstrate that separating the nucleation event from continuous growth and using the optimal conditions for each step is key to obtaining stable 2D sodium metal growth conditions.

1. Introduction

Sodium-ion batteries (SIBs) are considered to be important sustainable alternatives to lithium-ion batteries (LIBs).[1,2] This is mainly due to the higher abundance of sodium resources as well as the physicochemical similarities between these two alkali metals.[3,4] Even though SIBs can utilize LIB fabrication processes, there is still a need to develop competitive positive and negative electrode materials, as well as electrolytes, for SIBs.

While positive electrode materials for SIBs are reaching commercial production levels with layered metal oxide materials, polyanion-type materials, and Prussian blue analogs,[5–9] the negative electrode materials are much more limited. SIBs cannot utilize graphite, due to issues with the intercalation of Na^+ in the graphite structure. This has caused the emergence of less ordered soft and hard carbons able to accommodate sodium ions. However, they are still limited in terms of energy density and initial coulombic efficiency (CE).[10,11]

Sodium metal is the ideal SIB negative electrode material as it provides a very high capacity (i.e., 1166 mAh g^{-1}) and a very low electrode potential (i.e., −2.7 vs SHE). While studies on stable metal electrodes has been ongoing since the 1980's for lithium-metal batteries (LMBs),[12] research on sodium-metal batteries (SMBs) was initiated more recently.[13,14] At present, issues with inhomogeneous metal growth during the cycling significantly limit lithium- and sodium-metal electrodes from being commercially deployed. Localized 3D growth leads to brittle metal nanostructures (i.e., mossy sodium or sodium filaments) that cause excessive solid electrolyte interphase (SEI) formation and often yield dead metal structures as the connection to the base metal electrode is severed during cycling. This generally results in capacity losses and/or an increased risk of short-circuits.[14,15]

Extensive research has been performed to understand why lithium- and sodium-metal electrodes display the abovementioned inhomogeneous growth behavior. Several different hypotheses have been proposed throughout the years, giving rise to a multitude of strategies to counteract the underlying problem. These strategies can be considered to stem from three research fields, based on the underlying hypothesis that: i) an

M. Hosseinzadegan, L. Nyholm, G. Hernández, D. R Maibach
Department of Chemistry – Ångström Laboratory
Uppsala University
Box 538, Uppsala SE-751 21, Sweden
E-mail: meghdad.hosseinzadegan@kemi.uu.se; david.rehnlund@kemi.uu.se

F. Bauer
Institute of Applied Materials – Energy Storage Systems (IAM-ESS)
Karlsruhe Institute of Technology (KIT)
Hermann-von-Helmholtz-Platz 1
Eggenstein-Leopoldshafen, D-76344 Karlsruhe, Germany

D. R Maibach
Battery Division
Polestar R&D
Polestar Performance AB
Göteborg SE-405 31, Sweden

The ORCID identification number(s) for the author(s) of this article can be found under https://doi.org/10.1002/aenm.202503627

DOI: 10.1002/aenm.202503627

inhomogeneous SEI with spatial variations in the interfacial resistance causes localized 3D nanostructured metal growth, ii) the SEI is mechanically unstable with respect to the pressure due to the underlying metal growth, causing fractures in the SEI that lead to preferential 3D nanostructured metal growth and iii) the 3D metal deposition is caused by high current density hot spots on the electrode surface which promote a nanostructured metal morphology. Based on these hypotheses, several approaches have been proposed to control, suppress, or prevent dendritic growth during Li- and Na-metal electrodeposition. These include liquid electrolyte modification,[16–18] solid-state electrolytes (SSEs),[19] artificial electrode surface modification,[20–22] and electrochemical self-heating induced healing[23,24] and pretreatment strategies.[25,26]

One frequently used approach aimed at obtaining a more even electrochemical growth is to minimize the formation of local current density hot spots on the electrode surface. Many authors have attempted to decrease the local current density by increasing the electroactive surface area.[20,21] This has involved the manufacturing of metal electrodes that are either highly porous or have a 3D nanostructured surface. Such electrodes are, however, susceptible to agglomeration of lithium/sodium metal on the surface of the electrode. The reason for this is that the metal deposition is more likely to take place on the top surface of the electrode than within the pores of a porous or 3D-structured electrode. As a result, it becomes difficult to deposit metal homogeneously on porous or 3D-shaped electrodes.

An alternative strategy is to electrochemically activate the metal electrode surface by separating the nucleation, or pitting event, from the subsequent electrodeposition, or electrodissolution step. This approach has been utilized for lithium-metal electrodes by Rehnlund[25] et al., and Huang et al.[26] This electrochemical approach is based on the inclusion of a short high-overpotential reductive or oxidative pretreatment pulse prior to the galvanostatic electrodeposition or electrodissolution step. During electrodeposition, the reductive pretreatment pulse is used to generate a high number of small metal nuclei on the electrode surface. The presence of these nuclei, which then serve as the starting points during the subsequent galvanostatic electrodeposition step, significantly increases the likelihood of homogeneous metal growth and hence promote 2D metal electrodeposition. In the electrodissolution case, an oxidative pretreatment pulse can analogously be used to make a subsequent electrodissolution step more homogeneous and remove sodium layer by layer. The results of the abovementioned pretreatment pulse studies also indicate that the experimental conditions used in conventional experiments (i.e., without any pretreatment pulse) do not lead to the formation of a sufficiently large number of nuclei to support homogenous 2D growth on the entire electrode surface. The reason for this is that the overpotential is too low to promote the formation of a sufficiently high number of nuclei.[27] This leads to localized high electric fields causing (mainly) the few metal nuclei to grow, and thus a high probability for the attainment of 3D (rather than 2D) electrodeposition.[28] With the viability of this theory proven for lithium-metal batteries, and the increase in beyond lithium technologies, it would be beneficial to test if the same approach can be implemented for other alkali-metals.

The aim of this study is to determine if the electrochemical pretreatment strategies developed for lithium-metal batteries[25,26] can be adapted to enable 2D sodium growth. The sodium metal growth behavior is investigated in the presence of oxidative or reductive potentiostatic pretreatment pulses as well as a combination of such pulses. The experiments are designed to yield a high sodium nuclei density, and homogeneous sodium deposition based on the variation of the pulse amplitude, pulse duration, location of the pulse in the cycling scheme and the sodium hexafluorophosphate ($NaPF_6$) salt concentration in the electrolyte. The electrochemical results are compared with the results of surface morphology analyses (based on high-resolution scanning electron microscopy) combined with image analysis. The results show that pretreatment pulses can significantly hamper the generation of mossy sodium metal structures and promote 2D sodium metal growth, in good agreement with previous results obtained for lithium-metal electrodes.[25,26,29] This indicates that obtaining a high nuclei density is essential to obtaining 2D (i.e., planar) sodium metal growth.

2. Results and Discussion

To achieve 2D (i.e., planar) sodium metal growth it is important to understand the key moments during the first electrodeposition or electrodissolution cycle, and how these are affected by the inclusion of a pretreatment pulse. It is particularly important to understand why the overpotential may vary during chronopotentiometric (i.e., constant current) experiments and how this can affect the structure of the resulting metal surface. Based on such an improved understanding,[30–34] it should be possible to adapt and transfer electrochemical pretreatment protocols developed for lithium-metal electrodes[25,26] to sodium-metal electrodes.

In this work, oxidative and reductive pretreatment pulses were employed individually and in different combinations to compare their impact on the sodium growth conditions and the morphology of sodium-metal electrodes obtained during the first electrodeposition or electrodissolution cycle. The experiments were performed in electrolytes containing 0.1 or 1.0 M $NaPF_6$ in EC:PC (1:1 with 5 vol% FEC). An electrolyte containing 1.0 M $NaPF_6$ is commonly used to achieve the highest ion conductivity,[35] whereas lower sodium salt concentrations are expected to allow the use of higher electrodeposition or electrodissolution overpotentials and thereby higher sodium nuclei or pit densities, thus promoting 2D sodium metal growth.[27,36,37]

The amplitude and duration of the potentiostatic pretreatment pulses were first defined using a set of half-cycle experiments which are described in Section S1 and Figures S1–S5 (Supporting Information). The experiments included oxidative or reductive pretreatment pulses followed by the corresponding electrodissolution or electrodeposition step, respectively. Starting with the oxidative potentiostatic pretreatment pulses, the results showed an increased current density with increasing pulse amplitude from +1 to +4 V vs Na^+/Na (Figure S1, Supporting Information). The initial overpotential during the subsequent galvanostatic electrodissolution decreased with increasing pulse amplitude and duration and the lowest value was found for a 1000 ms long pulse with an amplitude of +4 V vs. Na^+/Na (Figure S2, Supporting Information). A lower initial overpotential indicates a smaller activation barrier for pit generation. Scanning electron

microscopy (SEM) analyses of the Na-metal electrodes after the first half-cycle showed a dramatic decrease in pit size when +4 V vs. Na^+/Na pretreatment pulses were applied, provided that the pulse length was at least 100 ms. It was also found that a homogenous and highly activated Na-metal electrode surface (seen as roughening of the surface in SEM) was obtained when using a +4 V vs Na^+/Na potentiostatic pretreatment pulse with a duration of 1000 ms (Figure S3, Supporting Information). For comparison, reductive pulses with amplitudes of −1 or −6 V vs Na^+/Na and a duration of 10 ms were used. During the pretreatment pulse an increased current density was seen with increasing pulse amplitude from −1 to −6 V vs Na^+/Na (Figure S4, Supporting Information). The lowest onset overpotential during the subsequent galvanostatic electrodeposition step was observed with the −6 V vs Na^+/Na pulse (Figure S5a,b, Supporting Information). SEM analyses showed a change from a localized mossy sodium deposit to a smooth hill-valley-like topography when using a −6 V vs Na^+/Na pulse rather than a −1 V pulse (Figure S5c–e, Supporting Information). Based on the pretreatment pulse design experiments, it was concluded that a short potentiostatic pulse with a high amplitude yielded the most homogenous electrodissolution or electrodeposition during the subsequent constant current step. Oxidative pulses of +4 V vs Na^+/Na with a duration of 1000 ms and reductive pulses of −6 V vs Na^+/Na with a duration of 10 ms were therefore used in the experiments discussed below. A relaxation time of 15 and 1 min at the open circuit voltage (OCV) was applied after the oxidative and reductive pulses respectively to allow the concentration gradient at the electrode/electrolyte interface to relax (for more details, see Section S1.3 and Figure S6, Supporting Information).

It should be noted that as the electrochemical data depended on the total electrode area, these data should have been relatively insensitive to the local changes in surface morphology of the electrodeposited metal. As a result, SEM images and the corresponding image analysis results (when feasible) were mainly used when studying the effect of the pretreatment pulse on the Na-metal electrode morphology. Reproducible patterns were, nevertheless, seen in the triplicate electrochemical data sets, and these patterns will therefore be compared with the SEM data below. Furthermore, potentiostatic electrochemical impedance spectroscopy (PEIS) measurements were performed to investigate the relation between the surface characteristics, the overpotential observed during galvanostatic cycling, and the interfacial impedance of the working electrode.

2.1. Single Oxidative Pulse Pretreatment

The experiments discussed in this section were performed to study the effect of a single oxidative potentiostatic pretreatment pulse on the subsequent galvanostatic cycling behavior and electrode morphology during the first cycle. The pretreatment pulse was followed by constant current cycling in the form of an electrodissolution step followed by an electrodeposition step. The analysis of the electrochemical data was supplemented by SEM image analyses. The working electrodes were extracted at the end of the electrodissolution step (i.e., cycle 0.5, shown in **Figure 1**) and at the end of the successive electrodeposition step (i.e., cycle 1.0, shown in **Figure 2**). The results of the electrochemical protocol without the oxidative pulse (i.e., protocol P1) was also compared with the results of the protocol with an oxidative pulse (i.e., protocol P2) using 0.1 M and 1.0 M $NaPF_6$-based electrolytes to study the effect of electrolyte concentration on the nucleation and growth behavior.

Figure 1 shows the electrochemical results, SEM images, and the corresponding image analysis data for the first electrodissolution step (cycle 0.5) performed with protocols P1 and P2 in 0.1 M and 1.0 M $NaPF_6$-based electrolytes. The protocols are schematically described in Figure 1a. In protocol P1, the cycling started with a galvanostatic electrodissolution with a current density and capacity of 1.0 mA cm^{-2} and 2.0 mAh cm^{-2}, respectively. In protocol P2, an oxidative potentiostatic pretreatment pulse (i.e., +4 V vs Na^+/Na for 1000 ms) was applied to the working electrode prior to galvanostatic electrodissolution, with the same parameters of the P1 protocol. Chronoamperograms for the oxidative pretreatment pulse applied in P2 (see Figure 1b) show a higher current density in the 1.0 M electrolyte compared to the 0.1 M electrolyte. This effect can be described by the lower solution resistance in the 1.0 M electrolyte (See Section S2 and Figure S7, Supporting Information).

The chronopotentiograms for the galvanostatic electrodissolution step in protocols P1 and P2 are shown in Figure 1c. In the 0.1 M electrolyte, the initial overpotential required to start the electrodissolution (see point 1) decreased from 580 mV vs Na^+/Na in P1 to 430 mV vs Na^+/Na in P2. This decrease was larger in the 1.0 M electrolyte, from 550 mV vs Na^+/Na in P1 to 300 mV vs Na^+/Na in P2. This indicates that the oxidative pulse pretreatment had a positive effect in decreasing the overpotential associated with the onset of sodium electrodissolution.

The electrodissolution chronopotentiograms also show that the overpotential dropped and then decreased with time to yield a steady state value, see e.g., point 2 and region 3 in Figure 1c. This behavior can be explained based on the initial need to form electrodissolution sites (e.g., pits) on the electrode surface which then grow, causing the overpotential to decrease. The chronopotentiograms obtained with the two protocols differed slightly, indicating differences in the pit growth behavior. Note the lower overpotentials for points 2 and region 3 in the 1.0 M electrolyte when using the P2 protocol demonstrating the beneficial effect of the oxidative pretreatment pulse approach even in the growth phase. The lower overpotentials obtained with the 1.0 M electrolyte than the 0.1 M electrolyte can mainly be ascribed to the larger solution resistance for the 0.1 M electrolyte (See Section S2, Supporting Information).

Figure 1d–g show the results of the SEM analyses performed on the sodium metal working electrodes at the end of electrodissolution step (i.e., cycle 0.5). With the P1 protocol (Figure 1d,f) a few pits were seen to be randomly located on an otherwise pristine sodium surface. This suggests that with the current density applied (i.e., 1 mA cm^{-2}) a few pits were formed on the inhomogeneously activated sodium metal surfaces, causing the pits to grow large and deep. However, with protocol P2 (Figure 1e,g), the entire surface appeared roughened at the end of the electrodissolution step. This roughening effect was more pronounced in the 1.0 M electrolyte than in the 0.1 M electrolyte. The higher magnification SEM image in Figure 1g shows that micrometer-sized pits, well distributed over the entire surface, were obtained in the 1.0 M electrolyte, whereas significantly larger pits were seen for

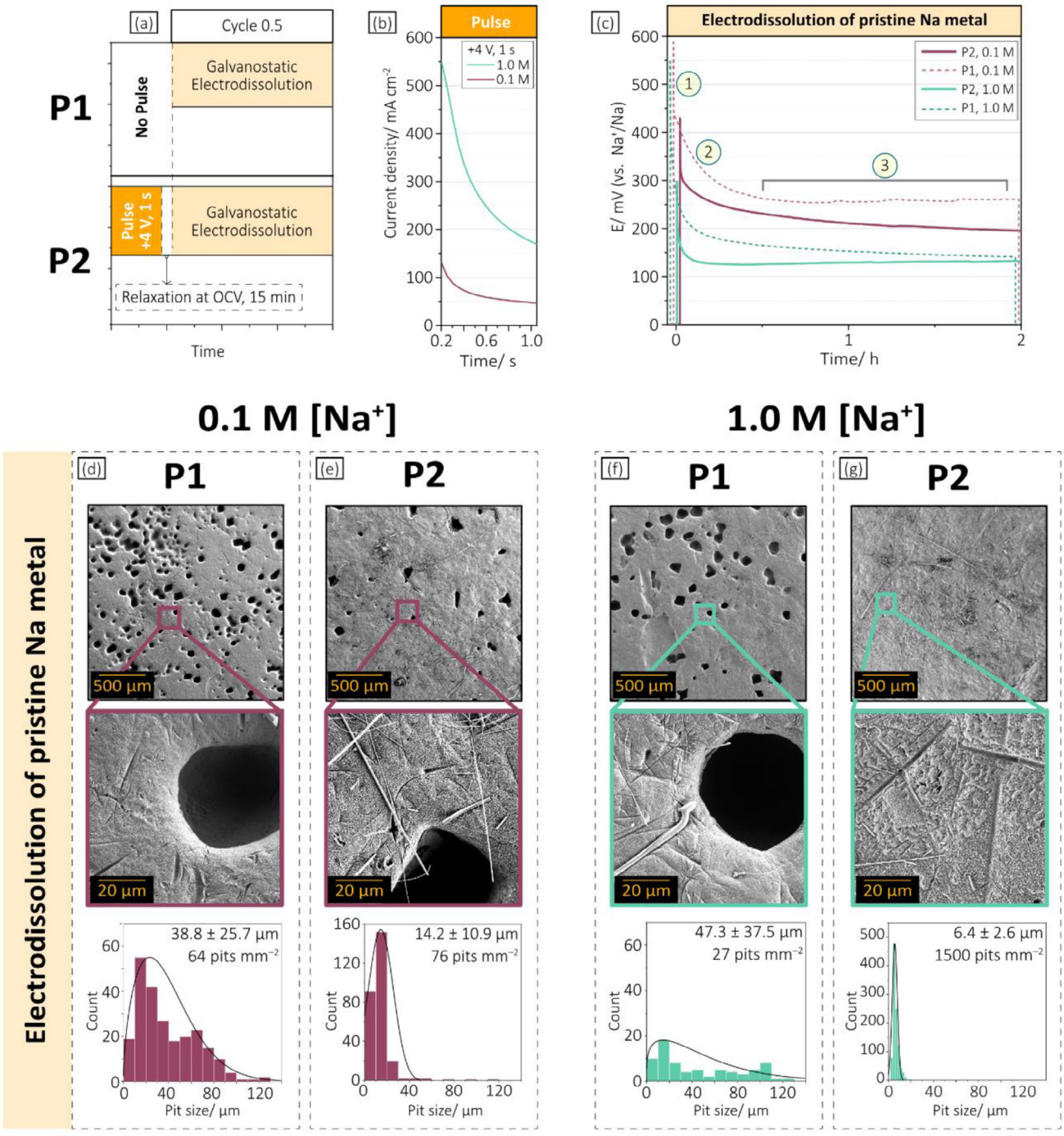

Figure 1. Schematic description of the P1 and P2 protocols for the 0.5 cycle (a), chronoamperograms for the oxidative pretreatment pulse applied in the P2 protocol (b), and chronopotentiograms obtained with the P1 and P2 protocols (c). SEM images taken using two different degrees of magnifications as well as the image analysis results after the galvanostatic electrodissolution step in the 0.1 M $NaPF_6$ electrolyte using the P1 (d), and P2 (e) protocols, and in the 1.0 M $NaPF_6$ electrolyte using the P1 (f), and P2 (g) protocols, respectively.

the 0.1 M electrolyte (even in P2), see Figure 1e. Additional visual evidence for the difference between pristine sodium metal as opposed to a roughened sodium surface with P2 is provided in Section S3 and Figure S8 (Supporting Information). This effect is also confirmed by Nyquist plots acquired at the end of the first electrodissolution step with and without a preceding oxidative pulse. As discussed later in Figure 4a, the interfacial impedance was significantly lower at the end of the first electrodissolution step when using a preceding oxidative pulse (i.e., in P2). This can be attributed to introduction of small well distributed pits

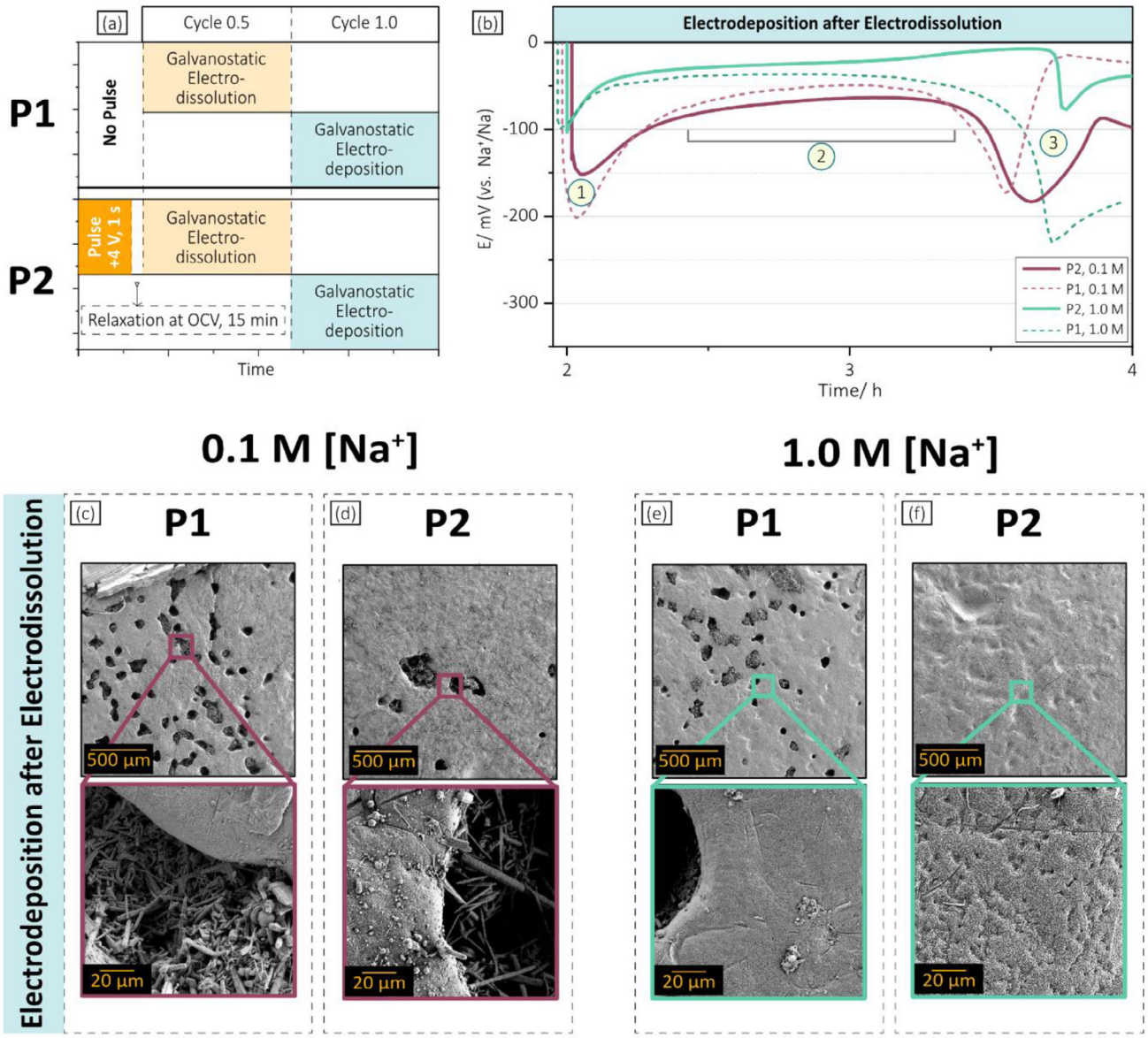

Figure 2. Schematic description of the P1 and P2 protocols for cycle 1.0 (a), chronopotentiograms obtained with the P1 and P2 protocols (b). SEM images taken with two different degrees of magnifications after the electrodeposition step in 0.1 M $NaPF_6$ with the P1 (c), and P2 (d) protocols and in 1.0 M $NaPF_6$ with the P1 (e), and P2 (f) protocols.

which increase the active surface area and decrease the interfacial impedance.

The results of the SEM image analysis (Figure 1d–g) show that applying an oxidative pretreatment pulse (i.e., protocol P2) caused the pit size to decrease and the pit frequency to increase in both electrolytes. In the 0.1 M electrolyte (Figure 1d,e), the average pit size (± standard deviation) decreased from 38.8 ± 25.7 µm in P1 to 14.2 ± 10.9 µm in P2 while the pit frequency increased from 64 in P1 to 76 pits mm^{-2} in P2. The same but more noticeable trend was observed in the 1.0 M electrolyte. Here, the average pit size decreased from 47.3 ± 37.5 µm in P1 to 6.4 ± 2.6 µm in P2, while the pit frequency increased from 27 in P1 to 1500 pits mm^{-2} in P2, see Figure 1f,g. This implies that the higher current density recorded during the potentiostatic oxidative pretreatment pulse in the 1.0 M electrolyte (Figure 1b) resulted in a more effective activation of the sodium surface, compared to when only using galvanostatic electrodissolution.

A comparison of the P1 protocol results obtained in the 0.1 and 1.0 M electrolytes (See average pit size and pit frequency values in Figure 1d,f) showed that the pit size was smaller while the pit frequency was higher for the 0.1 M electrolyte. This effect can be ascribed to the higher overpotential in the 0.1 M electrolyte during the initial phase of the electrodissolution step (Figure 1c, point 2), resulting in a higher number of smaller pits. The lower concentration electrolyte experienced a comparatively higher overpotential shift due to both an increased solution resistance

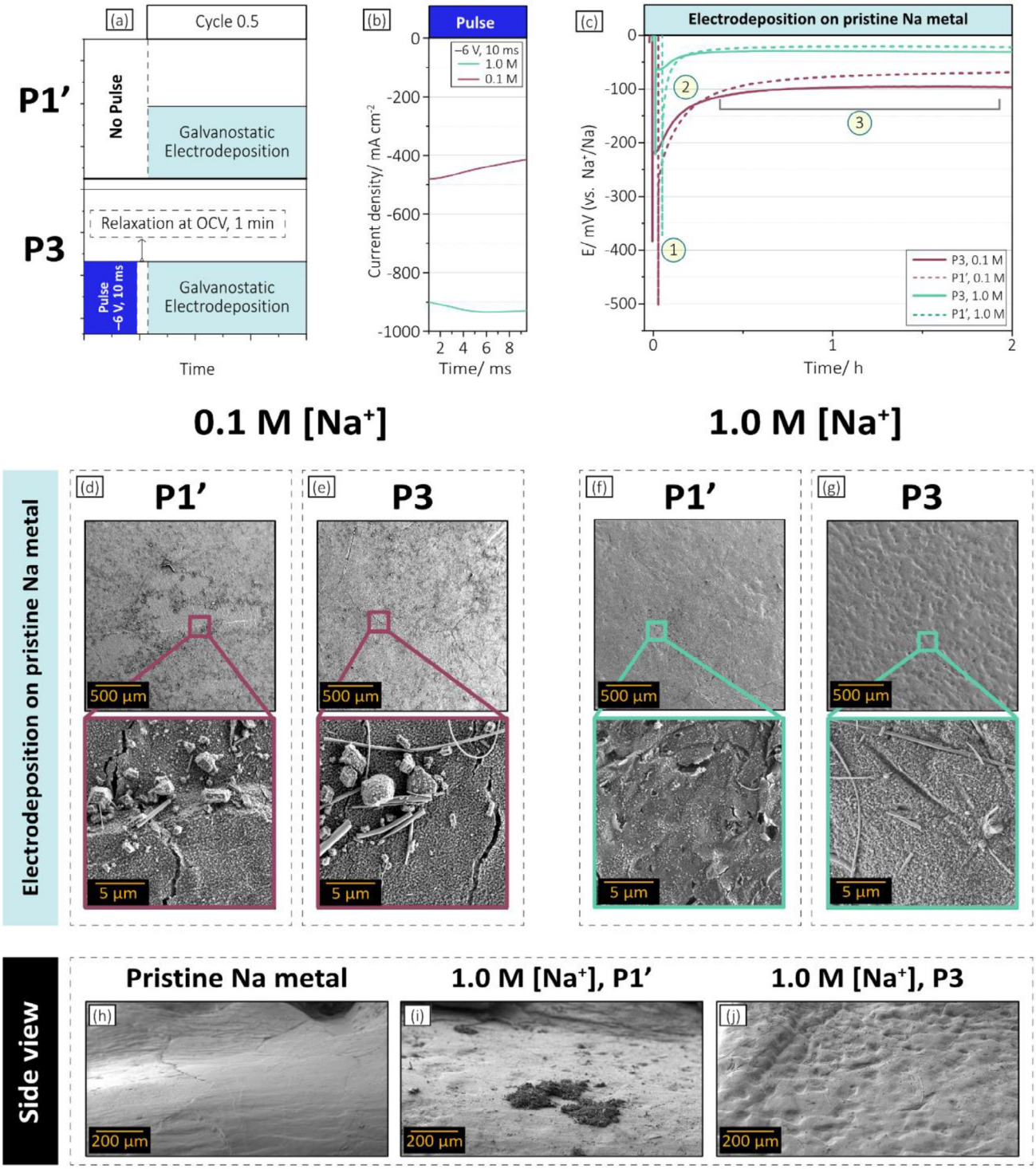

Figure 3. Schematic description of the protocols P1' and P3 (a), chronoamperograms for the reductive pulse applied in P3 (b), and chronopotentiograms obtained with the P1' and P3 protocols (c). SEM images taken using two different degrees of magnification after the galvanostatic electrodissolution step in the 0.1 M $NaPF_6$ electrolyte with the P1' (d), and P3 (e) protocols, and in the 1.0 M $NaPF_6$ electrolyte with the P1' (f), and P3 (g) protocols. Side-view SEM images of pristine sodium metal (h), sodium metal electrodeposition using the P1' (i), and P3 (j) protocols in 1.0 M $NaPF_6$.

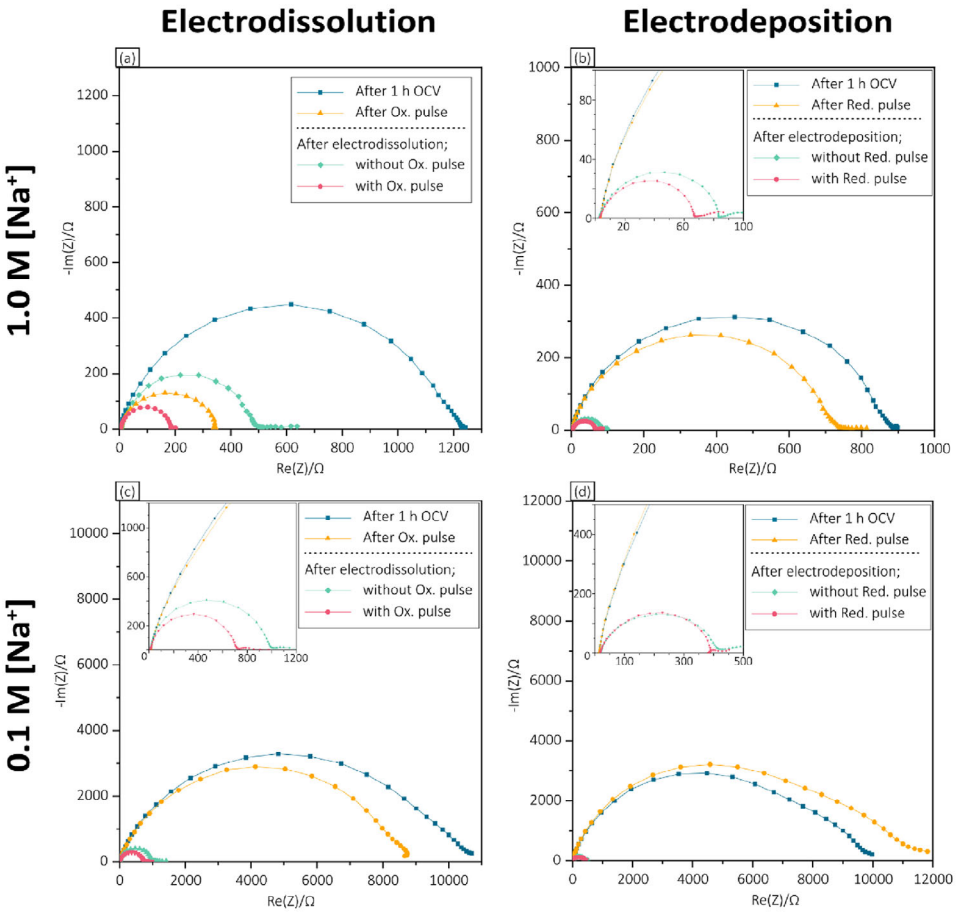

Figure 4. Nyquist plots representing PEIS results for working electrodes after selected steps during electrodissolution with and without an oxidative pulse (a,c), and electrodeposition with and without a reductive pulse (b,d) in 1.0 M (top row) and 0.1 M $NaPF_6$- based electrolytes (bottom row).

(i.e., from 250 Ω for 1.0 M electrolyte to 320 Ω for 0.1 M electrolyte, see Section S2, Supporting Information) and polarization effect. The latter is caused by the change in local Na^+ concentration at the working electrode during electrodissolution, that caused a more pronounced potential shift between the working and the reference electrode.

Figure 2 shows the results of the full cycle galvanostatic electrodissolution followed by electrodeposition, and the SEM images obtained at the end of the full cycle. Noticeably lower overpotentials (compared to the first electrodissolution step) were initially recorded for the P1 and P2 protocols in both the 0.1 M and 1.0 M electrolytes (Figure 2b, point 1). To understand this, it should be noted that the electrodeposition occurred after the electrodissolution step, which had formed pits on the sodium metal surface. These pits could hence act as preferential sites (i.e., edges, kinks, and steps) with lower activation energy barrier for sodium nucleation. Furthermore, this can be confirmed by the PEIS results shown in Figure 4a. It is evident that in all cases, the interfacial impedance at the end of the electrodissolution was lower than the pristine sodium surface (i.e., measured at OCV). A drop in overpotential was then seen when the growth was stabilized to yield steady state conditions (Figure 2b, region 2).

The sodium growth conditions were, however, not stable throughout the entire electrodeposition step as can be seen from the sudden increase in the overpotential (see Figure 2, point 3). This effect, which is often seen for alkali metal electrodes,[38] indicates that the metal deposition rate became too low to uphold the applied constant current density. A second nucleation event at a higher overpotential was therefore required to form new nuclei on the pristine electrode surface. Nyquist plots acquired before and after the overpotential spike (Figure S9, Supporting Information) add another dimension to explain this behavior. It is clear that the interfacial impedance of the working electrode, at the end of the electrodeposition step, was significantly higher than during steady state growth (i.e., before the overpotential spike). This indicates the presence of a high impedance surface structure made of mossy and tortuous sodium rather than low impedance freshly plated sodium.

A clear difference in the sodium surface morphology was observed with protocol P2 and 1.0 M electrolyte when comparing Figure 2c–e with Figure 2f. In the lower magnification image shown in Figure 2f, the surface exhibited a topography featuring smooth hill-valley-like topography. This was, however, not caused by the electrodissolution step removing base sodium but rather new sodium forming this morphology during the subsequent

electrodeposition step. It should be noted that no evidence for mossy sodium growth in pits nor as islands on the base electrode was found. This difference for P2 in 1.0 M compared with P1 in both concentrations, and P2 in 0.1 M, could likewise be observed in the chronopotentiograms (Figure 2b). During the electrodeposition, the steady state phase (region 2) was extended with the P2 protocol only in the 1.0 M electrolyte. This can be explained by the more densely populated pits that were formed during the P2 pretreatment pulse generating more activated sites for sodium growth. The same feature was not seen for P2 in 0.1 M electrolyte (compare Figure 2d,f), due to the higher iR drop discussed earlier (See Section S2, Supporting Information).

Overall, the single oxidative pretreatment pulse induced a large population of small pits that decreased the overpotential during subsequent galvanostatic sodium electrodissolution and electrodeposition. This resulted in a more homogenous sodium electrode surface morphology, especially in 1.0 M electrolyte. The SEM images for multiple samples (only one of which is discussed in this manuscript) showed that mossy sodium growth was more likely to happen at the edge of the big pits and not on the roughened containing well-distributed small pits.

2.2. Single Reductive Pulse Pretreatment

The next step was to study the influence of a reductive pretreatment pulse on the subsequent constant current electrodeposition step. Here a new reference protocol P1' (i.e., without any reductive pretreatment pulse) was introduced to be compared with the P3 protocol that included a reductive pretreatment pulse. Both protocols were studied in 0.1 and 1.0 M $NaPF_6$ electrolytes. These protocols as well as the electrochemical results and SEM images obtained after the electrodeposition step (i.e., cycle 0.5) are shown in **Figure 3**. Galvanostatic electrodeposition was carried out using a current density and capacity of 1.0 mA cm^{-2} and 2.0 mAh cm^{-2}, respectively, for both the P1' and P3 protocols. In protocol P3, a 10-ms-long reductive potentiostatic preconditioning pulse, with an amplitude of −6 V vs Na^+/Na was followed by a 1-min OCV pause.

During the potentiostatic reductive pulse in P3, a higher current density was recorded in the 1.0 M electrolyte compared to the 0.1 M electrolyte, see Figure 3b. This effect can be explained based on the lower iR drop in the 1.0 M electrolyte (See Section S2, Supporting Information). The chronopotentiograms of the galvanostatic electrodeposition step for the P1' and P3 protocols are shown in Figure 3c. The first notable difference between the results for the P1' and P3 protocols concerns the initial nucleation overpotential (point 1) in the 1.0 M electrolyte which decreased from −370 mV vs Na^+/Na in P1' to ≈−220 mV vs Na^+/Na in P3. The same trend was observed in the 0.1 M electrolyte where the overpotential decreased from −500 mV to −380 mV vs Na^+/Na. The lower nucleation overpotential seen with protocol P3 (compared to protocol P1') in both electrolytes can be ascribed to the effect of the pretreatment pulse. The initiation of the sodium growth (around point 2) also occurred at a lower overpotential with protocol P3. Steady state growth (region 3) then followed during which both P1' and P3 yielded similar overpotentials. The electrochemical data therefore indicate that the P3 reductive pretreatment pulse affected the sodium nucleation event. To better understand this effect, SEM imaging was conducted on all samples after the electrodeposition step (i.e., cycle 0.5), and these results are shown in Figure 3d–g. It should also be noted that the steady state growth overpotential values shown in Figure 3c, region 3 were comparable to the corresponding levels in Figure 2b, region 2. This suggests that starting the galvanostatic cycling with electrodeposition might be as beneficial and less complicated than starting with electrodissolution.

In the 0.1 M electrolyte (Figure 3d,e), islands of 3D sodium were observed at higher magnification for both P1' and P3, indicating that a homogeneous coverage of the base sodium surface by newly plated sodium was not achieved. With the 1.0 M electrolyte, the surface morphology was different (Figure 3f,g) as a smooth hill-valley-like topography was seen especially when using protocol P3. This is a surface topography which resembles planar deposition of sodium on the entire electrode surface (2D growth).

No decisive differences were seen between the results of the P1' and P3 protocols in the 1.0 M electrolyte based on the higher magnification images. Side-view SEM imaging was therefore performed to further probe the sodium surface morphology of pristine sodium electrodes as well as the used electrodes at the end of protocols P1' and P3 in the 1.0 M electrolyte (Figure 3h–j). Islands of mossy sodium were then clearly seen alongside an otherwise smooth surface in Figure 3i. The flat regions observed in P1' (Figure 3i) are clearly similar in morphology to the pristine sodium electrode surface (Figure 3h), therefore indicating that these regions were inactivated. In contrast, protocol P3 resulted in homogenous surface coverage with newly plated sodium yielding a smooth hill-valley-like topography. This morphology indicates that a majority of the electrode surface had been electroactive during the electrodeposition step. The difference is also confirmed by Nyquist plots acquired at the end of the electrodeposition step (**Figure** 4b). It is clear that the interfacial impedance at the end of the first electrodeposition was lower due to a preceding reductive pulse in 1.0 M electrolyte.

To explore the relation between surface characteristics and interfacial impedance, PEIS measurements were carried out. The experiments were performed with the same symmetrical pouch cell configuration. The PEIS measurements were performed in the selected steps, i.e. i) after 1 h at OCV, ii) after each oxidative or reductive pulse (when applicable), and iii) after electrodissolution or electrodeposition accordingly. Figure 4 shows the Nyquist plots recorded at each of the mentioned steps for protocols starting with electrodissolution (i.e., P1 and P2), and electrodeposition (i.e., P1' and P3) in 1.0 M and 0.1 M electrolytes. The oxidative pulse decreased the interfacial impedance of the sodium metal working electrode, an effect that was more noticeable in the 1.0 M electrolyte (Figure 4a) than the 0.1 M electrolyte (Figure 4c). Furthermore, a lower interfacial impedance was seen after the first galvanostatic step with an oxidative pulse applied beforehand. The impedance drop was larger in the 1.0 M electrolyte (Figure 4a) than the 0.1 M electrolyte (Figure 4c). This is in good agreement with the SEM and chronopotentiometry data shown previously in Figure 1, suggesting that the roughening effect of the oxidative pulse leads to introduction of well-distributed small pits on the surface of the working electrode, i.e., increasing the electro-active surface area, and thereby decreasing the impedance.

An understandably different trend was seen in the evolution of the interfacial impedance in the case of the reductive pulse and electrodeposition (Figure 4b,d). The reductive pulse did not significantly affect the impedance neither in the 1.0 M electrolyte (Figure 4b) nor in the 0.1 M electrolyte (Figure 4d). However, a significant drop in the impedance was observed after the first electrodeposition step in both electrolytes regardless of pretreatment pulse. This can be attributed to the presence of the freshly plated sodium. This effect has been studied for lithium metal,[39] where a better coverage of the electrode surface with accessible and porous freshly plated lithium decreased the impedance compared to that of the base lithium. When a reductive pretreatment pulse is applied in the 1.0 M electrolyte (Figure 4b inset), the impedance was further decreased after the electrodeposition step. This suggests that more of the electrode surface was covered with freshly plated sodium in the presence of the reductive pulse. This effect was not seen in the 0.1 M electrolyte (Figure 4d inset) which can be attributed to the ineffectiveness of the reductive pulse in the 0.1 M electrolyte. This is in good agreement with the SEM image shown in Figure 3e.

In summary, the single pulse pretreatment was seen to improve the electrochemical deposition of sodium metal to yield an improved surface morphology. The overpotential required for the nucleation or pitting, and in some cases also the steady state electrodeposition or electrodissolution, was decreased. A change in the surface morphology toward a homogenous and dense distribution of micrometer-sized pits and smooth undulating topography was seen as a result of the oxidative and reductive pulses, respectively. Even though the single pretreatment pulses were designed to affect their respective half-cycle (i.e., electrodissolution for the oxidative pulse and electrodeposition for the reductive pulse), their influence was clearly seen throughout the full cycle. In Figure 1g, it is seen that pits were formed during the oxidative pulse and electrodissolution step, and that this affected the morphology in the following electrodeposition step promoting a smooth hill-valley-like sodium growth (see Figure 2f) instead of mossy growth that was seen for the protocol without pretreatment in Figure 2c,e. In addition, this smooth hill-valley-like sodium growth is also seen in Figure 3g,j after a reductive pulse and electrodeposition step. PEIS measurements further showed that the effect of the pretreatment pulses decreased the interfacial impedance in good agreement with the data obtained from the SEM images and chronopotentiograms. To better understand this interplay and to continue the knowledge transfer from the lithium metal studies,[25–27,29] the effects of double pulse pretreatment was further investigated.

2.3. Double Pulse Pretreatment

It has so far been shown that the use of reductive or oxidative potentiostatic pretreatment pulses can improve the growth behavior of sodium metal by providing more well-controlled formations of pits or nuclei. To further explore the possibilities of the potentiostatic pretreatment pulses, double pulses in three different arrangements were employed in the 1.0 M $NaPF_6$-based electrolyte. In these experiments, the 0.1 M electrolyte was not used due to its higher solution resistance and hence larger iR drop.

2.3.1. First-Cycle Experiments

In **Figure 5**a, the double pulse pretreatment protocols P4, P5, and P6 (as well as the P1 protocol used for comparison) are schematically described. The electrochemical data and the SEM images of the electrode surface recorded after the last electrodeposition step are shown in Figure 5b–f, respectively. In the P4 and P5 protocols, the reductive and oxidative potentiostatic pretreatment pulses were applied prior to their respective electrodeposition or electrodissolution step while both pulses were combined as a pretreatment before the galvanostatic electrodeposition or electrodissolution step in the P6 protocol.

The effects of the P5 and P6 protocols starting with an electrodeposition step was first compared (see Figure 5b, frame 1 magnified). The double pulse applied at the beginning in the P6 protocol lowered the initial nucleation overpotential by ≈75 mV vs Na^+/Na compared to that of the P5 protocol. This difference can hence be ascribed to the oxidative pulse included prior to the reductive pulse in protocol P6. The oxidative pulse activated the sodium surface by creating small well-distributed pits (its effect on the electrodissolution was seen in Figure 1), which is why the subsequent reductive pulse became more effective. Consequently, the galvanostatic electrodeposition was initiated at a lower overpotential. Nevertheless, the single reductive pulse in the P5 protocol resulted in an ≈50 mV vs Na^+/Na lower overpotential for steady state growth compared to the double pulse used in the P6 protocol. This too can be explained by the presence of the small well-distributed pits in P6. During the electrodeposition in P6, the small pits continue to act as preferential sites for sodium nucleation. In other words, P6 showed more progressive growth behavior while P5 showed more instantaneous growth.[40]

In the subsequent electrodissolution step, the electrochemical results for P5 and P6 are shown using overlapping timeline with the first electrodissolution step for P1 and P4. As seen in frame 2 in Figure 5b, the initial pitting overpotentials observed for protocols P1 and P4 (600 and 200 mV vs Na^+/Na respectively) were largely removed with protocols P5 and P6 (50 mV vs Na^+/Na). The low overpotential suggests that the freshly deposited sodium rather than the original pristine sodium electrode was electrodissolved when using protocols P5 and P6. Moreover, steady state electrodissolution of freshly deposited sodium (using protocols P5 and P6) required a significantly lower overpotential (less than 30 mV vs Na^+/Na for P5 and P6) than electrodissolution of the base sodium (120–180 mV vs Na^+/Na for P4 and P1, respectively).

As shown in frame 3 in Figure 4b, at the end of the electrodissolution step a sharp increase in the overpotential was seen with protocols P5 and P6 yielding similar overpotentials as with protocols P1 and P4. This indicates a dramatic change in the sodium removal conditions. This pattern, which is often seen for lithium and sodium-metal electrodes, is typically ascribed to the generation of dead sodium as the mossy branches of the sodium detach from the base sodium electrode or become too thin and thereby too resistive to undergo further electrodissolution.[14,41] Consequently, an insufficient amount of plated sodium would remain to uphold the constant current density applied, which would require the formation of new pits on the base sodium. It was also observed that the abovementioned change in overpotential happened slightly later when using the P6 rather than the P5 protocol. This indicates that more plated sodium was available for

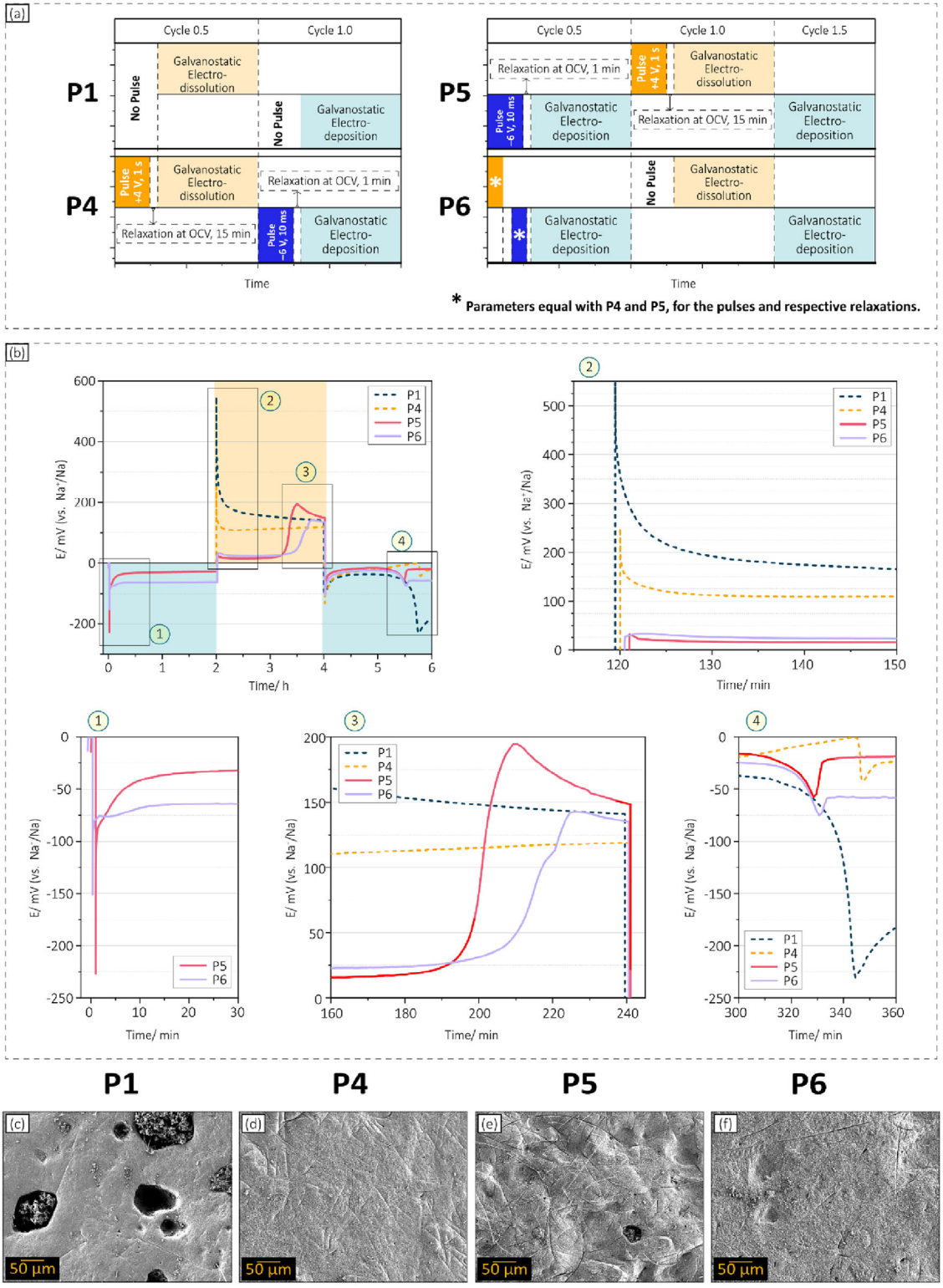

Figure 5. Schematic description of the P1, P4, P5, and P6 protocols (a), chronopotentiograms obtained with the P1, P4, P5, and P6 protocols (b), and SEM images obtained after the last electrodeposition step (with the P1, P4 after cycle 1.0, and P5, and P6 after cycle 1.5 protocols in 1.0 M $NaPF_6$ (c).

low overpotential electrodissolution (i.e., less mossy sodium was generated during the preceding electrodeposition) using the P6 compared to the P5 protocol. The difference in electrodissolution overpotential and its relationship with interfacial impedance is confirmed by the Nyquist plots acquired before and after the overpotential spike (Figure S9, Supporting Information) as is discussed in Section S4 (Supporting Information).

The results of the final electrodeposition step looked very similar at the early stage for all the protocols. However, the last stage, magnified in frame 4 in Figure 5b, showed some differences regarding the location and size of the overpotential spike for the four different protocols. For protocol P1 a larger (i.e., ≈−230 mV vs Na^+/Na) overpotential peak was seen compared to the pulse pretreatment protocols (i.e., protocols P4–P6, between −40 and −70 mV vs Na^+/Na). As discussed in Section 2.1, the change in the overpotential was due to insufficient access to nucleation sites to uphold the applied constant current density. The magnitude of the overpotential peak also indicates the presence of a large activation energy difference for the nucleation of sodium on a preferential site (e.g., at the edge of a pit, formed during the previous electrodissolution step) and on the pristine sodium surface. In contrast, the overpotential difference was much smaller with the P4–P6 protocols. This indicates that the surface was roughened and electrochemically activated as a result of the pulse pretreatment steps.

Clear differences can also be seen in the SEM images taken after the last electrodeposition step (see Figure 5c–f). With the P1 protocol large pits (i.e., 20–80 µm diameter), in which mossy sodium nanostructures could preferentially grow, were generated during the previous electrodissolution step. These mossy-sodium-filled pits were surrounded by inactivated pristine sodium metal. The double pulse protocols (i.e., protocols P4–P6) produced notably different surface morphologies. There was no evidence of any inactive pristine sodium as a roughened planar sodium metal surface was observed, indicative of 2D growth and activation of all pristine sodium. Although sporadically limited number of pits containing mossy sodium metal were observed with protocol P5, no such pits could be found with the P4 and P6 protocols. This difference could be due to the oxidative pulse being less effective in protocol P5 since this pulse was partially applied to the newly plated sodium rather than affecting only the base sodium surface.

Overall, the double pulse protocols P4–P6 improved the electrodeposition and electrodissolution conditions. This yielded a significant improvement in the sodium metal electrode morphology on the first cycle. To study if the effects of the pretreatment could also be seen during long-term cycling, further experiments were performed as will be described in the following section.

2.3.2. Long-Term Cycling and Full-Cell Configuration

As demonstrated above, potentiostatic pretreatment pulses can have a positive effect on the sodium growth behavior on sodium-metal electrodes during the initial cycles. To further study this effect, two sets of experiments were performed. First, long-term cycling of symmetrical Na||Na cells was examined. In these experiments the results of three double pulse protocols (i.e., protocols P4, P5 and P6) were compared with those of the reference protocols P1 and P1'. Second, the protocols were tested in full-cell configuration with sodium metal as the anode and Prussian white as the cathode to explore the practical feasibility of the pulse protocols.

Figure 6 combines the results for symmetrical Na||Na cells with full-cell experiments. For the symmetrical Na||Na cells, the chronopotentiograms for the working electrode from a representative cell are presented in Figure 6a, and the number of cycles reached before failure for all the cells tested and the mean cycle number are shown in Figure 6c. For full-cell experiments, chronopotentiograms of the sodium metal as the anode are demonstrated in Figure 6b, while the CE of the full-cells cycled with different protocols is shown in Figure 6d. It should be noted that for full-cell experiments, only protocols which included galvanostatic electrodeposition as the first step (i.e., P1', P5, and P6) were tested to comply with the real-world battery applications and pave the way for later studies on anode-less systems.

As seen in Figure 6a, between cycle 10 and 12, all protocols displayed essentially the same type of profiles with minor differences regarding the overpotentials. This similarity intensified as the long-term cycling continued, thus suggesting that the sodium became similar during long-term cycling in symmetrical Na||Na cells. Comparing the chronopotentiograms for cycles 10 to 12 with those for cycles 43–48, the steady state potential increased, and the overpotential spike decreased as the long-term cycling continued (i.e., d_2 is smaller than d_1). In other words, the rise from steady state pitting overpotential to the second overpotential became smaller. This indicates that several layers of plated sodium metal were accessible (instead of the base sodium metal) for further electrodissolution to uphold the applied constant current. The same type of evolution holds true for the electrodeposition. This suggests that the surface tortuosity increased during the cycling.

The results shown in Figure 6c for symmetrical Na||Na cells suggest no remarkable improvement during long-term cycling for any of the protocols. Protocols P5 and P6, which included galvanostatic electrodeposition as the first step, had longer mean cycle life (i.e., 152 and 194 cycles, respectively) than the P4 (i.e., 53 cycles) which started with galvanostatic electrodissolution. However, quantitatively there was no significant difference between any of the protocols since the cell-to-cell variation was too large. This can be attributed to the contribution of the counter electrode (which provides the required current density for all the electrochemical events happening on the working electrode) as its surface was consequently affected in an uncontrollable manner. Since the long-term cycling experiments of symmetrical Na||Na cells did not show any conclusive results, full-cell experiments were performed to assess the behavior of the protocols in a more realistic environment closer to the final application.

Figure 6b shows the evolution of the sodium anode potential during three different stages of cycling in a full-cell configuration. The steady state overpotentials were lower compared to those for the symmetrical cells and they were more stable both during charge (sodium electrodeposition) and discharge (sodium electrodissolution). Another difference shown in Figure 6b compared to Figure 6a is that no overpotential spike or obvious bump was observed during final stage of charge (sodium electrodeposition) in the full-cell experiments. This suggests that the overpotential increase observed at the end of

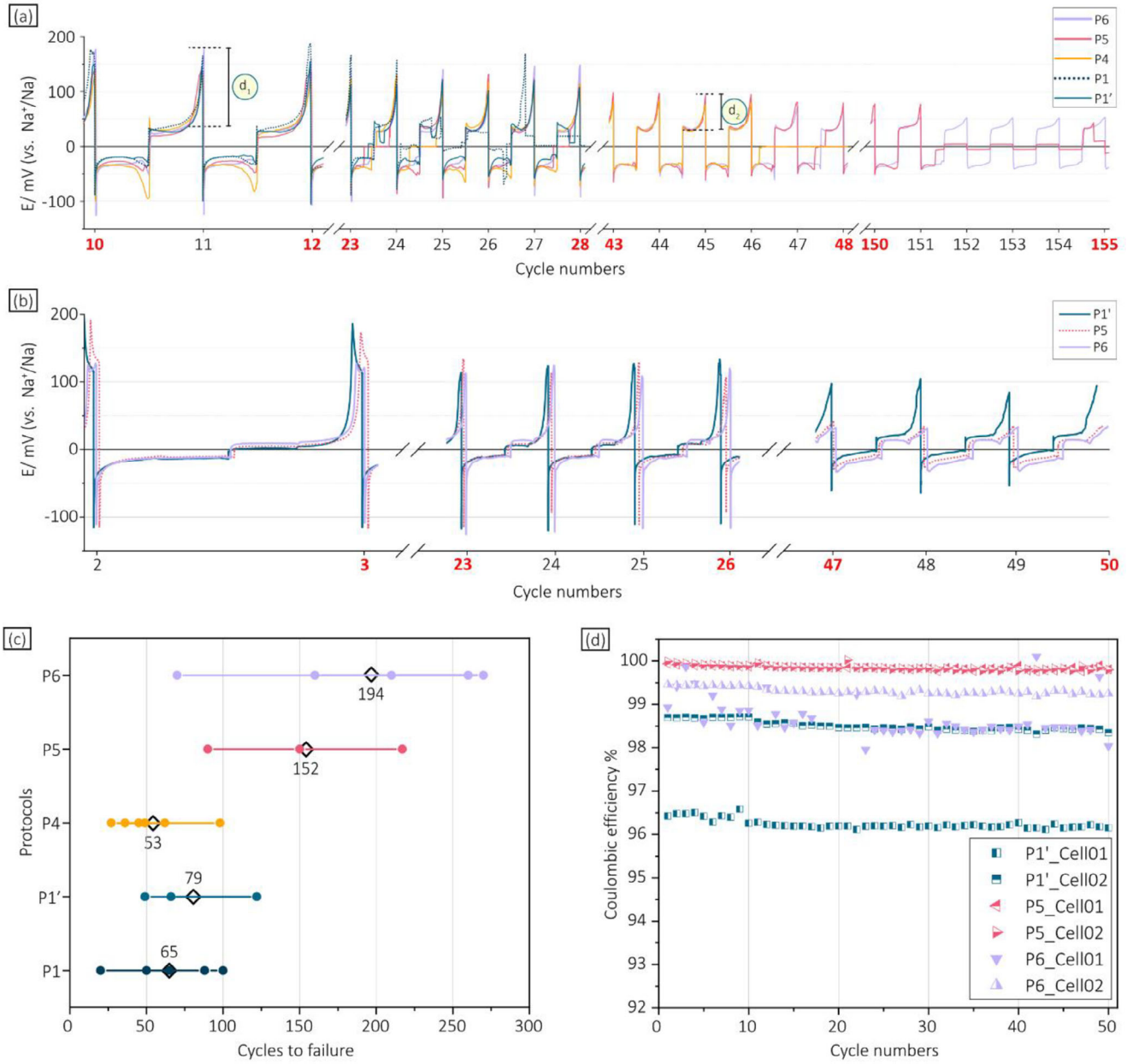

Figure 6. Long-term cycling results for symmetrical Na||Na cells and full-cell experiments for the double-pulse treatment protocols (P4, P5, and P6) and the reference (no-pulse) cycling protocols (P1 and P1'). Chronopotentiograms of the working electrode at various stages of the long-term cycling of symmetrical Na||Na cells (a), Chronopotentiograms of sodium anode in full-cell setup in various stages with different protocols (b), number of cycles reached with symmetrical Na||Na cells with at least three cells for each protocol and the mean value (c), and coulombic efficiency of two full-cells for the different protocols(d).

electrodeposition in symmetrical Na||Na cells was caused by the sodium metal counter electrode.[42] In other words, during the final stages of electrodeposition on the working electrode, the counter electrode experiences final stages of electrodissolution simultaneously, i.e., electrodissolution of base sodium metal occurs. This stage has always shown a high overpotential which is attributed to higher impedance of electrodissolving the inactivated base sodium metal, as confirmed by the PEIS measurements. As seen in Figure S9b (Supporting Information), the interfacial impedance increased roughly 30-fold at the end of the electrodissolution stage when compared with that for the steady state electrodissolution.

Cycling of full-cells is assessed based on the CE as it is related to the electrodeposition and dissolution of the sodium metal. Figure 6d shows the CE of two cells per each protocol for the first 50 cycles. Protocol P5 showed the highest and most consistent CE between the two samples (99.89% and 99.92%). However, while P6 showed higher CE (99.07% and 99.43%) compared to P1' (96.43% and 98.75%), it turned out to be unstable (i.e., P6_Cell01). This suggests that any type of

electrodissolution event (i.e., oxidative pulse in P6) before the first galvanostatic electrodeposition step might be detrimental to the stability of the sodium metal growth in the long run, as seen as well with the wide range of cycle life in symmetrical cells.

The long-term cycling results in the symmetrical Na||Na cells showed that starting with an electrodissolution event damaged the sodium surface regardless of the pretreatment pulses, and generally lead to shorter cycling stability of sodium-metal electrodes (P1, P4, and P6). Nevertheless, contribution of the counter electrode with a maltreated surface complicates the interpretation of long-term cycling experiments involving symmetrical cells. Furthermore, the first-cycle pretreatment effect was gradually lost during the long-term cycling as the chronopotentiograms looked more and more similar. Despite the benefits of the double pulses observed in the first cycle, the 2D nucleation and growth could not be maintained, at least not with the studied electrolytes. This indicates that the 2D deposition is imperfect and requires more levers of control to be maintained during long term cycling. Full-cell experiments showed promise at least in the initial 50 cycle period with P5 showing indications of stable cycling with highest CE among other protocols. However, full-cell experiments with different electrolytes and with anodeless configuration seems necessary, which is currently under investigation.

3. Conclusion

In this study, it is demonstrated that the initial nucleation or pitting event can be selectively activated and thereby separated from the growth/removal phase by applying short high-overpotential potentiostatic pretreatment pulses, enabling 2D sodium metal growth.

The reductive and oxidative potentiostatic pulses used in the pretreatment of the sodium-metal electrodes were found to significantly decrease the overpotential for electrodeposition and electrodissolution, which resulted in more stable cycling conditions. The oxidative pulse created a rich population of small pits across the entire electrode surface which stabilized the growth behavior of sodium metal. The reductive pulse likewise improved the growth conditions for sodium by yielding 2D growth that resulted in an undulating smooth hill-valley-like topography. With the pretreatment pulses, nanostructured mossy sodium deposits were avoided although they were seen without pulse pretreatment. Both pulses reduced the interfacial impedance at the end of the corresponding first step (i.e., reductive pulse for first electrodeposition and oxidative pulse for first electrodissolution). The oxidative pulse had the most significant effect by introducing higher surface area of activated metal, hence decreasing the interfacial impedance.

Combining the reductive and oxidative pulses can significantly limit the generation of mossy sodium and large pits during the first cycles. However, the order of the pulse during the first cycle was found to be important. While an oxidative/reductive pulse pair (Protocol P6) can greatly improve the electrodeposition step, applying the oxidative pulse alone prior to electrodissolution (Protocol P4) makes the cells prone to early failure since the densely pitted surface can trigger intensive deep pitting and nanostructured mossy growth during long-term cycling. Furthermore, an oxidative pulse applied after the first galvanostatic electrodeposition (Protocol P5) makes the pulse less effective due to division of the current density between newly plated sodium and base sodium metal. This on the other hand proved to be beneficial in the full-cell configuration as P5 showed highest CE with the highest reproducibility. Unstable cycling of full-cells with P6 protocol showed the adverse effect of pitting on the pristine sodium surface, even in the form of a short oxidative pulse.

The results hence show that short high-overpotential potentiostatic pulses can be used to effectively pretreat sodium-metal electrodes. This is done by separately activating the nucleation and pitting events using other conditions than those of constant current steady state growth or removal of sodium. This important finding opens up a myriad of opportunities to further study electrochemical pretreatment strategies to develop high-performing and safe sodium metal negative electrodes. While the findings presented in this study represent an important step forward, the smooth hill-valley-like sodium growth could not be maintained during long-term cycling. These fundamental questions must be answered using several additional methods such as X-ray photoelectron spectroscopy (XPS) in the future works. The preliminary results on full-cell configuration paves the way for our next steps toward an anode-less system. There are several additional aspects of the technology that can and should be further developed such as pulsed galvanostatic cycling protocols as well as designing electrolytes with the purpose of promoting 2D sodium metal electrodeposition/electrodissolution. Pulsed galvanostatic cycling could prevent adverse effects of the concentration gradient, while electrolyte design can help with long-term stability of the cells and mitigation of sodium ion migration. A comprehensive approach is then needed to achieve stable, efficient, and safe sodium-metal batteries.

4. Experimental Section

Three-electrode symmetrical pouch cells with sodium metal as working electrode, counter electrode and reference electrode were used in the experiments to study the surface evolution of sodium metal. In the full-cell experiments, three-electrode pouch cells with sodium metal as working electrode and reference electrode, and Prussian white as counter electrode were used. Sodium metal (Sigma–Aldrich, 99.9% trace metal basis) was pressed onto aluminum foil substrates and the electrodes were punched and cut from the pressed foil. In the symmetrical cell configuration, the working and counter electrodes were punched into pieces with 10- and 12-mm diameters respectively, whereas the reference electrodes were cut to yield small stripes with arbitrary shapes. Inside the pouch cell (containing three aluminum current collector tabs), the working electrode was placed facing the reference and counter electrodes. Two layers of separators were placed between the working and counter electrodes, as the reference electrode was partially inserted in-between the two separators. In full-cell configuration, the working electrode (sodium metal) and counter electrode (Prussian white) were punched into pieces with 16- and 15-mm diameters respectively. The counter electrodes were supplied by Altris and had a Prussian white mass loading of 24 mg cm^{-2} (theoretical capacity 150 mAh g^{-1}). Two layers of glass fiber separators (Whatman glass microfiber grade GF/A, 260 µm thickness) were soaked with 200 µL electrolyte. The experiments were performed in two electrolytes composed of 0.1 M and 1.0 M sodium hexafluorophosphate ($NaPF_6$, Fluorochem, ≥99.99%) in a mixture of propylene carbonate (PC, Gotion, ≥99.98%, water content ≤20 ppm) and ethyl carbonate (EC, Gotion, ≥99.95%, water content ≤20 ppm), (EC:PC, 1:1 v) with 5 vol % fluoroethylene carbonate (FEC, Sigma–Aldrich, ≥99%, anhydrous) as an additive. The water content of the electrolytes was measured by the Karl Fischer titration method (Metrohm) to ensure a residual water content less than 20 ppm. Electrode manufacturing,

electrolyte preparation, and cell assembly was performed inside an inert atmosphere argon-filled glovebox with O_2 and H_2O values less than 1 ppm.

The electrochemical protocols were applied to the pouch cells using a multichannel Biologic VMP–2 potentiostat. The oxidative pulse was a potentiostatic pulse of +4 V vs Na^+/Na applied for 1000 ms, while the reductive pulse was a potentiostatic pulse of −6 V vs Na^+/Na applied for 10 ms. The potentiostatic pulses were followed by a pause at the OCV for 15 and 1 min for oxidative and reductive pulses respectively, to allow the concentration gradient at the electrode/ electrolyte interface to relax (see Section S1.3, Supporting Information). The galvanostatic cycling steps were performed with a current density of ±1 mA cm^{-2} until a capacity of 2 mAh cm^{-2} was reached. PEIS measurements were performed in the 10 mHz to 1 MHz frequency range with an ac amplitude of 2.0 mV using three-electrode symmetrical sodium cells. The PEIS experiments were done after a 10-min rest at the OCV after each electrochemical step, to assure acquisition of data at equilibrium.

The surface morphologies of the sodium electrodes were studied with high-resolution SEM (Merlin, Zeiss). The sample preparation was performed by carefully removing the sodium working electrode from the disassembled cell inside the glovebox and washing it with dimethyl carbonate (DMC) to remove any residual salt, electrolyte degradation products, and excess electrolyte. The electrodes were then dried for at least 2 h under vacuum conditions at room temperature in the glovebox (either in a Büchi oven or the antechamber) to ensure complete evaporation of the washing solvent from the electrode. The electrodes were then mounted on SEM stubs and transferred to the SEM chamber under inert atmosphere using a specialized air-tight SEM transfer shuttle (Semilab). The SEM images were obtained with an Inlens detector as well as a high efficiency secondary electron (HE-SE) detector with 3.0–5.0 KeV acceleration voltage and a beam current varying from 70 to 120 pA to avoid charge accumulation on the sample surface. The working distance (WD) was kept nearly constant to achieve good comparison between samples, apart from rare cases of side-view imaging were the WD was increased to have a wider focus range. Image analysis of the pit size distribution was performed with the open-source Image J software using the following procedure: 1) Adjust the contrast; 2) Set the scale according to SEM scale bar; 3) Process the image with FFT function and bandpass filter; 4) Apply the threshold function to convert the image to binary; 5) Analyze the particle size; 6) Transform the areal data to pit diameter; 7) Plot the histograms and summarize the data.

Supporting Information

Supporting Information is available from the Wiley Online Library or from the author.

Acknowledgements

The authors acknowledge Altris for providing the Prussian white electrodes. The authors would also like to acknowledge Dr. Charles Aram Hall and Jan Felix Schuster for valuable discussions. The Swedish Energy Agency is acknowledged for funding this research project (P2021-90018). COMPEL and the Swedish Strategic Research Program STandUP for Energy are acknowledged for financial support. The authors acknowledge Myfab Uppsala for providing facilities and experimental support. Myfab is funded by the Swedish Research Council (2020-00207) as a National Research Infrastructure.

Conflict of Interest

The authors declare no conflict of interest.

Data Availability Statement

The data that support the findings of this study are available from the corresponding author upon reasonable request.

Keywords

dendritic growth, electrodeposition, energy storage, sodium-metal batteries

Received: July 1, 2025
Revised: August 29, 2025
Published online:

[1] A. Mahmoudzadeh Andwari, A. Pesiridis, S. Rajoo, R. Martinez-Botas, V. Esfahanian, *Renew. Sustain. Energy Rev.* **2017**, *78*, 414.
[2] P. C. K. Vesborg, T. F. Jaramillo, *RSC Adv.* **2012**, *2*, 7933.
[3] L. Zhao, T. Zhang, W. Li, T. Li, L. Zhang, X. Zhang, Z. Wang, *Engineering* **2023**, *24*, 172.
[4] J.-M. Tarascon, *Joule* **2020**, *4*, 1616.
[5] B. Wang, Y. Han, X. Wang, N. Bahlawane, H. Pan, M. Yan, Y. Jiang, *iScience* **2018**, *3*, 110.
[6] M. H. Han, E. Gonzalo, G. Singh, T. Rojo, *Energy Environ. Sci.* **2014**, *8*, 81.
[7] T. Jin, H. Li, K. Zhu, P.-F. Wang, P. Liu, L. Jiao, *Chem. Soc. Rev.* **2020**, *49*, 2342.
[8] L. N. Zhao, T. Zhang, H. L. Zhao, Y. L. Hou, *Materials Today Nano* **2020**, *10*, 100072.
[9] N. Hong, S. Zhang, J. Li, H. Wang, J. Huang, X. Hu, B. Zhang, F. Hua, J. Zeng, W. Jian, C. Sun, N. Bugday, W. Deng, G. Zou, H. Hou, Z. Hu, Z. Long, Y. Wu, X. Ji, *Angew. Chem., Int. Ed.* **2025**, *64*, 202423479.
[10] Y. Liu, B. V. Merinov, W. A. Goddard, *Proc. Natl. Acad. Sci. USA* **2016**, *113*, 3735.
[11] P. K. Nayak, L. Yang, W. Brehm, P. Adelhelm, *Angew. Chem.* **2018**, *57*, 102.
[12] S. Kim, G. Park, S. J. Lee, S. Seo, K. Ryu, C. H. Kim, J. W. Choi, *Adv. Mater.* **2023**, *35*, 2206625.
[13] S. Wang, B. Peng, J. Lu, Y. Jie, X. Li, Y. Pan, Y. Han, R. Cao, D. Xu, S. Jiao, *Chem. Eur. J.* **2023**, *29*, 202202380.
[14] B. Lee, E. Paek, D. Mitlin, S. W. Lee, *Chem. Rev.* **2019**, *119*, 5416.
[15] J. Conder, C. Villevieille, *Chem. Commun.* **2019**, *55*, 1275.
[16] K. Naoi, M. Mori, Y. Naruoka, W. M. Lamanna, R. Atanasoski, *J. Electrochem. Soc.* **1999**, *146*, 462.
[17] Y.-S. Hong, N. Li, H. Chen, P. Wang, W.-L. Song, D. Fang, *Energy Storage Mater.* **2018**, *11*, 118.
[18] L. Schafzahl, I. Hanzu, M. Wilkening, S. A. Freunberger, *ChemSusChem* **2017**, *10*, 401.
[19] A. Hayashi, K. Noi, A. Sakuda, M. Tatsumisago, *Nat. Commun.* **2012**, *3*, 856.
[20] R. Zhang, X.-B. Cheng, C.-Z. Zhao, H.-J. Peng, J.-L. Shi, J.-Q. Huang, J. Wang, F. Wei, Q. Zhang, *Adv. Mater.* **2016**, *28*, 2155.
[21] Y. Lu, Q. Zhang, M. Han, J. Chen, *Chem. Commun.* **2017**, *53*, 12910.
[22] H. Tu, Y. Zhang, J. Wu, Y. Li, H. Liu, W. Deng, G. Zou, H. Hou, X. Ji, *Adv. Funct. Mater.* **2025**, *35*, 2413488.
[23] L. Li, S. Basu, Y. Wang, Z. Chen, P. Hundekar, B. Wang, J. Shi, Y. Shi, S. Narayanan, N. Koratkar, *Science* **2018**, *359*, 1513.
[24] P. Hundekar, S. Basu, X. Fan, L. Li, A. Yoshimura, T. Gupta, V. Sarbada, A. Lakhnot, R. Jain, S. Narayanan, Y. Shi, C. Wang, N. Koratkar, *Proc. Natl. Acad. Sci. USA* **2020**, *117*, 5588.
[25] D. Rehnlund, C. Ihrfors, J. Maibach, L. Nyholm, *Mater. Today* **2018**, *21*, 1010.
[26] Y.-K. Huang, R. Pan, D. Rehnlund, Z. Wang, L. Nyholm, *Adv. Energy Mater.* **2021**, *11*, 2003674.
[27] A. Pei, G. Zheng, F. Shi, Y. Li, Y. Cui, *Nano Lett.* **2017**, *17*, 1132.
[28] J. O'M Bockris, M. Gamboa-Aldeco, A. K. N. Reddy, **2002**, https://doi.org/10.1007/b113922.

[29] A. Aleshin, S. Bravo, K. Redquest, K. N. Wood, *ACS Appl. Mater. Interfaces* **2021**, *13*, 2654.
[30] A. J. Sanchez, E. Kazyak, Y. Chen, K.-H. Chen, E. R. Pattison, N. P. Dasgupta, *ACS Energy Lett.* **2020**, *5*, 994.
[31] J. Steiger, D. Kramer, R. Mönig, *J. Power Sources* **2014**, *261*, 112.
[32] J. Steiger, D. Kramer, R. Mönig, *Electrochim. Acta* **2014**, *136*, 529.
[33] A. Kushima, K. P. So, C. Su, P. Bai, N. Kuriyama, T. Maebashi, Y. Fujiwara, M. Z. Bazant, J. Li, *Nano Energy* **2017**, *32*, 271.
[34] C. Fang, J. Li, M. Zhang, Y. Zhang, F. Yang, J. Z. Lee, M.-H. Lee, J. Alvarado, M. A. Schroeder, Y. Yang, B. Lu, N. Williams, M. Ceja, L. Yang, M. Cai, J. Gu, K. Xu, X. Wang, Y. S. Meng, *Nature* **2019**, *572*, 511.
[35] D. Rehnlund, F. Lindgren, S. Böhme, T. Nordh, Y. Zou, J. Pettersson, U. Bexell, M. Boman, K. Edström, L. Nyholm, *Energy Environ. Sci.* **2017**, *10*, 1350.
[36] M. Paunovic, M. Schlesinger, *Fundamentals of Electrochemical Deposition*, John Wiley & Sons, Ltd, Hoboken, NJ, USA, **2006**.
[37] G. Oltean, L. Nyholm, K. Edström, *Electrochim. Acta* **2011**, *56*, 3203.
[38] R. Rodriguez, K. E. Loeffler, S. S. Nathan, J. K. Sheavly, A. Dolocan, A. Heller, C. B. Mullins, *ACS Energy Lett.* **2017**, *2*, 2051.
[39] S. Drvarič Talian, G. Kapun, J. Moškon, R. Dominko, M. Gaberšček, *Nat. Commun.* **2025**, *16*, 2030.
[40] E. R. Cooper, M. Li, I. Gentle, Q. Xia, R. Knibbe, *Angew. Chem., Int. Ed.* **2023**, *62*, 202309247.
[41] A. J. Sanchez, N. P. Dasgupta, *J. Am. Chem. Soc.* **2024**, *146*, 4282.
[42] J. R. Fitzpatrick, B. E. Murdock, P. K. Thakur, T.-L. Lee, S. Fearn, A. J. Naylor, D. Biswas, N. Tapia-Ruiz, *Adv. Sci.* **2025**, *12*, 04717.